Rev #1

Effects of Surface Heterogeneity y on Thermal Remote Sensing of Land Parameters

E. G. Njoku[1], S. J. Hook[1], and A. Chehbouni[2]

[1] Jet Propulsion Laboratory
California Institute of Technology
4800 Oak Grove Drive
Pasadena, California 91109, USA

[2] ORSTOM
Laboratoire d'Hydrologic
911 Avenue Agropolis, B.P. 5045
34032 Montpelier, France

Submitted for publication in the Proceedings of the Workshop on Scaling Up Hydrological Variables using Remote Sensing

to be held at the
Institute of Hydrology, Wallingford, UK
June 10-12, 1996

Jet Propulsion Laboratory
California Institute of Technology
Pasadena, California

September, 1995

Abstract

In this paper, simplified radiative transfer models and two-component simulations are used to illustrate the effects of surface heterogeneity on remotely sensed land parameters in the thermal infrared and microwave spectral regions, The regions considered are 9-12 μm in the infrared, and 3-24 cm in the microwave, The simulations show that remote sensing observations over heterogeneous terrain yield estimates of sensor-averaged, or "effective", parameters that may be significantly different from the area-averaged, or "composite", parameters that are often assumed to be estimated by the remote sensors. Differences as large as 0.4 'C in surface temperature, 0,01-0.06 g cm^{-3} in surface soil moisture, and 0.2-1.0 kg m^{-2} in vegetation water content, or larger, may be common. These differences arise from different sources in the infrared and microwave domains, but are a result in both cases of the nonlinear radiative transfer relationships between surface parameters and radiance received by the sensor. In the infrared case, for surface temperature, the nonlinearity is caused by the Planck function, In the microwave case, the nonlinearity is caused primarily by the vegetation opacity, such that the effective surface temperature, surface soil moisture, and vegetation water content always differ from their composite counterparts when vegetation is present. The magnitude of these differences depends on wavelength, the nonlinearities increasing in both infrared and microwave regions as the wavelengths decrease. The differences also depend on the relative fractional covers of the components and On their parameter contrasts, typically being largest at intermediate values of fractional cover, In many situations, the differences between effective and composite surface parameters may be small and can be safely neglected. However, in some cases, particular in semiarid environments or agricultural areas where large parameter contrasts exist between bare and vegetated surfaces, unexpectedly large differences may occur that need to be addressed. The use of visible and near-infrared sensing to obtain information on "within-pixel" fractional vegetation cover should be considered in these cases.

1. Introduction

Remote sensing observations, used in conjunction with in situ measurements, can provide information of value in modeling and monitoring the biophysical processes governing balances of energy and water at the land surface. <observations from space are uniquely suited to studying the spatial and temporal variabilities of these processes over a wide range of scales due to their wide-swath mapping and orbital sampling capabilities. Knowledge of the fluxes of energy and water at the surface, the manner in which these fluxes are affected by changing atmospheric and surface characteristics, and the way they vary in different climatic regimes is important, since the fluxes represent boundary conditions for dynamical models of atmospheric circulation and water movement in the soil (Bougeault (1991), Famiglietti et al. (1992)). The fluxes are also important controlling influences in dynamical models of ecosystem functioning and crop growth (Running (1 990), LoSeen et al. (1 995)).

A number of important issues must be addressed in the use of remote sensing observations as inputs for the development and operation of these models. Parameterizations of surface characteristics and fluxes must be matched to parameterizations of radiative transfer. This requires formulation of relationships between the parameters of the biophysical and observational models and methods to interpolate their different space-time sampling. The sensitivities of the models to their descriptive parameters must be assessed, so that assimilation methods may be developed that are resistant to the effects of uncertainties and noise inherent in the observational data, and in order to select optimal channel configurations and develop retrieval methods for maximum information transfer. Remote sensing observations must be considered as an adjunct to, not as a replacement for, in situ data in such studies.

In addressing linkages between surface fluxes and remote sensing observations, most studies either assume spatial homogeneity (single component) within the remote sensor footprint (pixel), or they assume that tile observations are related to area-weighted averages of the surface parameters ("composite" parameters), in which the weights are the fractional coverages of the different surface types. The implications of these assumptions have not been adequately investigated. Thus, studies using thermal infrared sensing to retrieve surface temperatures (Wan and Dozier (1989), Becker and

Li (1990), Sobrino et al. (1991), Kerr et al. (1 992), Prata (1993), and Kealy and Hook(1 993)), and to obtain surface fluxes (e.g. Kustas et al. (1 989), Holwill and Stewart (1 992)), have commonly assumed that surface temperature and emissivity are constant within the observation pixel (~1 -km dimension from space). Similarly, in studies of vegetation and soil moisture using passive microwave sensing, homogeneous or area-weighted surface parameters are usually assumed within the footprint (Choudhury et al. (1987), Owe et al. (1992)). However, land surfaces exhibit significant heterogeneity at all spatial scales, and the coupling of radiation from different surface components into the sensor receiving aperture, as expressed by the radiative transfer and sensor reception equations, is nonlinear. Hence, unexpected biases may occur in retrievals of surface parameters and fluxes using remotely sensed data if these heterogeneities are not investigated and understood. In many cases these biases may be negligible; in some they may be unacceptably large. Recent investigations have begun to address these aspects and to quantify the extent of naturally-occurring heterogeneity (Dozier (198 1), Caselles and Sobrino (1989), Labed and Stoll (1991), Becker and Li (1994), Humes et al. (1994)).

In this paper we use a simplified approach to investigate the effects of surface heterogeneity on thermal infrared and microwave remote sensing observations, and on the pararneterizations by which they are linked to land surface energy fluxes. Most rough soil and vegetated surfaces impose a three-dimensional heterogeneity at the land-atmosphere interface. However, for our purposes we shall consider only the two-dimensional heterogeneity of the radiation field just above the soil or vegetation, thus avoiding consideration of radiation interactions within the volume or cavities of the surface. The discussion is somewhat idealized, but nevertheless can be used to illustrate the magnitudes of the effects of interest. To illustrate the effects, a variety of two-component surfaces are simulated with parameters ranging over extents typical of some natural surfaces. The wavelength regions considered are 9-12 μm in the infrared, and 3-24 cm (10-1 .25 GHz) in the microwave, since these are the regions most commonly used for thermal sensing of land parameters.

In Section 2 simplified surface energy and radiative transfer parameterizations are presented as a context for describing how parameters derived from thermal remote sensing data may be used in estimating fluxes. In Section 3 the expressions for remotely sensed "effective" parameters are presented and compared with the expressions for composite temperature. In Section 4 simulations are performed using

two-component surfaces to indicate the magnitudes of nonlinearities potentially introduced in parameter retrievals due to effects of heterogeneity. Section 5 contrasts the expressions for remotely sensed effective parameters with those developed to represent large-area surface fluxes, and Section 6 presents the conclusions of the study.

2. Model Parameterizations

The two basic challenges to be addressed in assimilating remote sensing data into hydrologic and atmospheric circulation models are: (1) defining appropriate parameterizations for linking the remote sensing and surface flux models so that the remotely sensed data can provide information directly to the models of biophysical processes in the soil and atmosphere; and (2) accounting for the differences in spatial and temporal resolutions at which the remote sensing measurements are made and at which the models of processes in the soil and atmosphere operate, This is particularly important in regions of strong surface heterogeneity, where high spatial and temporal variability of surface fluxes occur, such as are often encountered in semiarid and some agricultural environments. Such environments are important for study, since they cover a large fraction of the globe, and significant a proportion of the human population depends on them for survival. Adverse climate change or surface degradation in these regions can have critical impacts on food and water supplies. Errors in remote sensing and flux modeling caused by ignoring the effects of surface heterogeneity are largest in these regions.

The focus of this paper is to illustrate the effects of heterogeneity primarily from a remote sensing viewpoint, thus the issue of determining appropriate parameterizations for aggregating surface fluxes over heterogeneous terrain is not addressed here (see for example Chehbouni et al. (199s)). However, the basic expressions for surface energy fluxes are provided below as a starting point to illustrate the manner in which remote sensing parameterizations are related to parameterizations of surface fluxes,

2.1 Surface Flux Parameterizations

A useful summary of surface flux parametrization schemes applicable to climate and hydrologic modeling is provided by Rowntree (1991). The energy flux boundary conditions are expressed by the surface energy balance equation:

$$R_n = H + LE + G \tag{1}$$

where, R_n is the net downward radiation flux at the surface, H and LE are the upward sensible and latent heat surface fluxes, respectively, (the latent heat flux LE is the product of the evaporative moisture flux E and the latent heat of vaporization L), and G is the downward heat flux into the soil. Units are in W m^{-2}.

Assuming a homogeneous, single interface, the following expressions may be used to describe the energy fluxes (Brutsaert (1 984), Rowntree (1991)):

$$R_n = (1 - \alpha) R_s + \varepsilon (R_l - \sigma T_s^4) \quad (2)$$

$$H = \rho C_p \left(\frac{T_s - T_a}{r_a} \right) \quad (3)$$

$$LE = \frac{\rho C_p}{\gamma} \left[\frac{e^*(T_s) - e_a}{r_a + r_s} \right] \quad (4)$$

$$G = \left(\lambda_g \frac{\partial T(z)}{\partial z} \right)_{z=0} \quad (5)$$

In these expressions, R_s and R_l are, respectively, the downward shortwave (solar) and longwave (thermal atmospheric) radiation at the surface, α and ε are the (broadband) shortwave albedo and longwave emissivity, respectively, (corresponding to R_s and RI), and σ is the Stefan-Boltzmann constant. p and C_p are the air density and specific heat at constant pressure, respectively, T_s is the surface temperature, T_a and e_a are the temperature and vapor pressure of the air, respectively, at a reference height z above the surface, and r_a is the atmospheric (or "aerodynamic") resistance to transfer from the surface (soil or vegetation) to the atmosphere, defined with respect to height z. γ is the psych rometric constant, $e^*(T_s)$ is the saturated vapor pressure at temperature T_s, r_s is the surface resistance to transfer from the soil (or the stomatal resistance in the case of vegetation), λ_g is the soil conductivity, and T(z) is the soil temperature profile (z positive upwards).

In Eqs. 2-5 the surface temperature T_s appears explicitly as a parameter. However, for many vegetated and heterogeneous surfaces it is difficult to define this temperature precisely. If the remotely sensed infrared (or "radiative") skin surface temperature is used for T_s then the definition of r_a must be adjusted accordingly by including a supplementary resistance to heat transfer (Prevot et al, (1994)). Since the microwave-derived surface temperature represents a deeper layer in the surface

(Njoku (1995)), a different modification to the resistance definition may be necessary in this case.

Soil moisture enters into the flux equations less explicitly, either in simplified expressions for the latent heat flux, or in more detailed treatments through expressions for the surface resistance r_s. According to the surface cover type and environmental conditions, the surface resistance includes dependence on atmospheric water vapor deficit, surface soil moisture, and water availability in the root zone. Various parameterizations of the surface resistance, involving soil moisture in the shallow surface layer and in the deeper root zone layer, have appeared in the literature (Rowntree (1991), Bougeault (1991). Microwave remote sensing can provide information directly on soil moisture in the surface layer (~1 cm). For bare soils, moisture in the deeper layers may be obtained indirectly from the surface soil moisture by combining surface measurements with a soil heat and moisture flux model (Entekhabi et al. (1994)). For vegetated soils, there does not appear to be a straightforward relationship between vegetation water content, as measured by a microwave radiometer, and soil moisture in the root zone. However, the vegetation water content may be a useful parameter in helping specify the fractional vegetation cover, and for monitoring vegetation growth, in climate and ecosystem models.

2.2 Radiative Transfer Parameterizations

The thermal spectral radiance from the Earth, $I_{\lambda o}$, as observed by a spaceborne sensor at infrared or microwave wavelengths, can be expressed as:

$$I_{\lambda o} = \exp(-\tau_\lambda) \{ \varepsilon_\lambda B_\lambda(T_s) + [1 - \varepsilon_\lambda] I_\lambda{\downarrow} \} + I_{\lambda a} \qquad (6)$$

where, the subscript λ is the wavelength and refers to spectral quantities. $I_{\lambda a}$ is the upwelling atmospheric radiance, τ_λ is the atmospheric opacity, and ε_λ is the surface emissivity, (all directional quantities in the viewing direction of the sensor). $I_\lambda{\downarrow}$ is the downwelling atmospheric radiance (assumed isotropic for simplicity), and $B_\lambda(T_s)$ is the blackbody radiance at surface temperature T_s. (The term $\exp(-\tau_\lambda)$ is often written as the "transmittance", particularly in infrared sensing. However it is written here in terms of "opacity" for consistency with usage elsewhere in microwave modeling), Eq. 6 is valid for a non-scattering atmosphere (aerosol- and cloud-free), and assumes azimuthal isotropy. (Dependence on 6, the zenith viewing angle, is understood). Ideally the expression should be integrated over the detector bandwidth centered at

wavelength λ, but this effect is small and will be ignored in this analysis. The Planck function, Ill(T'), is given by the expression:

$$B_\lambda(T) = \frac{C_1}{\pi\lambda^5[\exp(C_2/\lambda T) - 1]} \qquad (7)$$

where, $C_1 = 2\pi hc^2$ (= 3.74183 x 10^{-16} W m^{-2}) and $C_2 = hc/k$ (= 1.43879 x 10^{-2} m K) are radiation constants, (h and k are Planck's and Boltzmann's constants, respectively, and c is the speed of light), λ and T are in units of m and K, respectively, and $B_\lambda(T)$ is in units of W m^{-2} m^{-1} sr^{-1} (Goody and Yung (1989)).

The spectral, directional emissivity, ε_λ, is not the same as the emissivity ε appearing in Eq. 2, which is equivalent to ε_λ integrated over the upper hemispherical solid angle, and over the broad thermal infrared spectral region. However, these quantities are often assumed to be the same, and for some surfaces the difference is indeed small. However, insufficient data exists to characterize this fully for many naturally occuring surfaces. Measurements of infrared emissivity have been reported in the literature both using laboratory samples and in natural environments (Salisbury and D'Aria (1992), Hipps (1989), van de Griend et al. (1991), and Labed and Stoll (199])). (The laboratory measurements are usually done in reflectance and have to be converted to emissivity, and the field measurements must be corrected for stray radiation artifacts. Thus, both procedures contain some measurement uncertainties.) Typical values range from about 0.9-0.96 for bare soils to about 0.985 for vegetation in the 9-12 μm waveband.

In the microwave region, the emissivity of bare soil, $\varepsilon_{\lambda s}$, decreases approximately linearly as a function of the soil water content, m, in the top 1-2 cm of soil, i.e.:

$$\varepsilon_{\lambda s} = \varepsilon_{\lambda o} + a_\lambda (m - m_o) ; \qquad (m \geq m_o) \qquad (8)$$

where, $\varepsilon_{\lambda o}$ and m_o are the emissivity and moisture content of dry soil, respectively, and a_λ is the slope of the emissivity-soil moisture relationship (a_λ takes negative values). $\varepsilon_{\lambda o}$ and a_λ are functions of wavelength, known by measurement and through their dependence on the dielectric constant of water, and depend also on the polarization of the radiation (vertical or horizontal). A more complete description of the relationships between soil moisture, dielectric constant, and emissivity, for smooth and rough surfaces, and soils of different textures, is given in Njoku and Entekhabi (1995). Eq. 8, though approximate, suffices for our purpose here. Representative

values for m_o, $\varepsilon_{\lambda o}$, and a_λ in the wavelength range 3-30 crn are available from measurements reported in the literature. In this study we shall use the following values, typical of a smooth, sandy loam soil, at horizontal polarization, and 20° zenith viewing angle (Wang et al. (1983)): m. = 0.0S g cm^{-3}, $\varepsilon_{\lambda o}$ = 0.87, and a_λ = -1.5 g-l cm^3. The emissivity can be seen to range, under these assumptions, from a high of approximately 0.87 for a dry soil, to a low of less than 0.S for a wet soil (m = 0.3 g cm^{-3}).

When vegetation is present, it may be modeled at long microwave wavelengths as a uniform, non-scattering layer above the soil. Assuming that the soil is at the same temperature as the overlying canopy, the emissivity of the vegetation-plus-soil medium, $\varepsilon_{\lambda c}$, may be expressed as:

$$\varepsilon_{\lambda c} = 1 - \exp(-\tau_{\lambda c}) [\, 1 - \varepsilon_{\lambda s} \, 1 \tag{9}$$

where, $\tau_{\lambda c}$ is the canopy opacity, which depends linearly on the vegetation water content WC (kg m^{-2}):

$$\tau_{\lambda c} = bW_c/\cos\theta \tag{lo}$$

The dependence of the coefficient b on wavelength and vegetation type is subject to some uncertainty. However, measurements indicate that b varies approximately inversely with wavelength, and is not highly dependent on vegetation type. A value of b = 0.1 $kg^{-1}m^2$ at λ = 20 cm is typical (Jackson and Schmugge (1 991)). Eqs. 9 and 10 show that the presence of vegetat ion above the soil increases the surface emissivity from the value for bare soil to a value of ~1 when the vegetation is very dense. (The single scattering albedo of the vegetation reduces this slightly, but is ignored here (Kerr and Wigneron (1995)). Values of WC range typically from approximately 0.5 kg m^{-2} for grass to 5.o kg m^{-2} for dense crops and >10 kg m^{-2} for forests.

3. Remotely Sensed Effective Parameters

Effective parameters have been proposed as a means for applying equations developed for homogeneous or point-scale processes to processes occuring at larger spatial scales over heterogeneous surfaces. Thus, for example, Shuttleworth (1991), Chehbouni et al. (1995), and others have studied the use of effective parameters in representing energy flux processes over heterogeneous surfaces, One method for deriving expressions for the effective parameters is to express the energy balance

equation separately in terms of effective and component surface parameters, and then to match the expressions term by term using some initial assumption about which fluxes will be "conserved" in going from the small to the large scale. The assumptions of which fluxes or parameters are conserved, and uncertainties as to whether the forms of the bulk parameterization equations remain valid at large scales over heterogeneous terrain, lead to some ambiguity in interpreting such effective parameters. However, much insight can be obtained by this method into the effects of aggregating nonlinear processes to larger scales.

A similar aggregation procedure can be used in applying the radiative transfer equation over large scales, In this case the situation is more clearcut since radiometer receiver theory defines how the radiation from a heterogeneous surface is aggregated as it is measured by the radiometer. This has recently been discussed by Becker and Li (1 994). Following this approach, the observed radiance from a heterogeneous surface is expressed as the solid angle weighted average, $\bar{I}_{\lambda o}$, of the radiance from each of the N components of the surface within the observed pixel or footprint:

$$\bar{I}_{\lambda o} = \sum_{i=1}^{N} \xi_i I_{\lambda o_i} \tag{11}$$

where, $\xi_i = (d\Omega_i/\Omega)$ is the fractional cover of component i, $d\Omega_i$ is the solid angle subtended by component i at the sensor, Ω is the solid angle subtended by the entire pixel at the sensor, and the fractional covers satisfy the constraint: $\sum_{i=1}^{N} \xi_i = 1$. $I_{\lambda o_i}$ are the radiance components at the horizontal two-dimensional plane just above the surface (thus avoiding consideration of radiation interactions within the cavities of the rough or vegetated surface). Strictly speaking, the expression for the weights ξ_i should include the effects of the sensor angular reception characteristics (i.e. the antenna pattern for a microwave radiometer). However this additional effect is ignored here, and it is assumed that the weights can be computed directly from the horizontal spatial areas of the surface components and pixels in the two-dimensional horizontal plane, and the zenith viewing angle. Applying Eq. 11 to Eq. 6 we obtain:

$$\bar{I}_{\lambda o} = \exp(-\tau_\lambda) \{ \sum_{i=1}^{N} \xi_i \varepsilon_{\lambda i} B_\lambda(T_{si}) + [1 - \sum_{i=1}^{N} \xi_i \varepsilon_{\lambda i}] I_\lambda{\downarrow} \} + I_{\lambda a} \tag{12}$$

where it is assumed that the atmosphere is homogeneous over the pixel.

The radiance observations $\bar{I}_{\lambda o}$ are normally used in remote sensing retrieval algorithms to estimate the sensor-averaged or "effective" emissivity and temperature over the pixel, $\bar{\varepsilon}_\lambda$ and $\bar{T}_s$, using an expression equivalent to Eq. 6, i.e:

$$\bar{I}_{\lambda o} = \exp(-\tau_\lambda) \{ \bar{\varepsilon}_\lambda B_\lambda(\bar{T}_s) + [1 - \bar{\varepsilon}_\lambda] I_\lambda{\downarrow} \} + I_{\lambda a} \tag{13}$$

Thus, from a remote sensing retrieval point of view, the following relationships between component and effective parameters are defined by matching terms in Eqs. 12 and]3:

$$\bar{\varepsilon}_\lambda = \sum_{i=1}^{N} \xi_i \varepsilon_{\lambda i} \tag{14}$$

and,

$$\bar{\varepsilon}_\lambda B_\lambda(\bar{T}_s) = \sum_{i=1}^{N} \xi_i \varepsilon_{\lambda i} B_\lambda(T_{si}) \tag{15}$$

or, equivalently, using Eq. 7:

$$\bar{T}_s = (C_2/\lambda) \left\{ \ln \left[1 + \frac{\bar{\varepsilon}_\lambda (C_1/\pi\lambda^5)}{\sum_{i=1}^{N} \xi_i \varepsilon_{\lambda i} B_\lambda(T_{si})} \right] \right\}^{-1} \tag{16}$$

In the microwave region of the spectrum, and for temperatures characteristic of Earth radiation, the Rayleigh-Jeans approximation ($hc << \lambda kT$) is valid, so that for a given wavelength the blackbody radiance is linear in temperature. In this case, Eq. 16 takes the simpler form:

$$\bar{T}_s = \frac{1}{\bar{\varepsilon}_\lambda} \sum_{i=1}^{N} \xi_i \varepsilon_{\lambda i} T_{si} \tag{17}$$

In the microwave region, we can take the analysis of emissivity a step further by combining Eqs. 8-10 to get:

$$\&_A = 1 - \exp[-bW_c/\cos\theta] [1 - \varepsilon_{\lambda o} - a_\lambda(m - m_o)] \tag{18}$$

and thus, using Eq. 14:

$$\bar{\varepsilon}_\lambda = 1 - [1 - \varepsilon_{\lambda o} + a_\lambda m_o] \sum_{i=1}^{N} \xi_i \exp[-bW_{ci}/\cos\theta] + a_\lambda \sum_{i=1}^{N} \xi_i m_i \exp[-bW_{ci}/\cos\theta] \quad (19)$$

The modeled sources of heterogeneity in this case are the soil moisture and vegetation water content. Other sources of heterogeneity such as soil texture, surface roughness, and vegetation type also play a role, but their effects are considered secondary here. From Eqs. 18 (treating the parameters as effective parameters) and 19, and matching terms as before, we find:

$$\overline{W_c} = -\frac{\cos\theta}{b} \ln \left\{ \sum_{i=1}^{N} \xi_i \exp[-bW_{ci}/\cos\theta] \right\} \quad (20)$$

and,

$$\overline{m} = \frac{\sum_{i=1}^{N} \xi_i m_i \exp[-bW_{ci}/\cos\theta]}{\exp[-bW_c/\cos\theta]} \quad (21)$$

Eqs. 14, 16, 17, 20, and 21 are the derived expressions for remotely sensed effective parameters. It can be seen that only in the case of emissivity are the effective parameters simple averages of the component parameters weighted by their fractional coverage areas as is often assumed. Except for emissivity, the weights are also functions of wavelength. This means that for multichannel retrieval algorithms, the weights for the retrieved effective parameters will be a combination of those at each wavelength. Furthermore, since microwave sensors often have different footprint sizes at different wavelengths, the type and magnitude of surface heterogeneity observed at each wavelength may be different. Also, in a more detailed analysis, the effects of heterogeneity should be evaluated in the context of atmospheric and sensor noise, so that the manner in which these influence the effects of heterogeneity in the retrievals may be assessed.

In the simulations of the next section, we restrict the discussion to two-component surfaces (i.e. N = 2), and allow the characteristics of the component surfaces to vary over realistic ranges. No constraints are provided on the independent variability of the surface parameters or on the juxtaposition of surface types as might be desired in a more realistic simulation. (However, the combinations of surface types used are quite representative of natural conditions.) The intent is to investigate the magnitudes of the nonlinear effects of heterogeneity, and to place bounds on these effects. It is of

most interest to examine the differences between the effective parameters $\overline{p}$, (where $\overline{p}$ may represent $\overline{\varepsilon_\lambda}$, $\overline{T_s}$, $\overline{W_c}$, or $\overline{m}$), and those which would be obtained if an area-weighted average were applied - referred to as "composite" parameters. We therefore define composite parameters, $\overline{p}^*$, by the expression:

$$\overline{p}^* = \sum_{i=1}^{N} \xi_i p_i \tag{22}$$

and examine, via simulation, the difference quantities:

$$\Delta\overline{p} = \overline{p} - \overline{p}^* \tag{23}$$

4. Simulations

4.1 "temperature and Emissivity

The simulated surface pixel is considered to be made up of two components, of fractional surface areas ξ_1 and $\xi_2 (=1-\xi_1)$, at temperatures T_{s1} and T_{s2}, and with emissivities $\varepsilon_{\lambda 1}$ and $\varepsilon_{\lambda 2}$, respectively. The fractional cover ξ_1 is varied from O to 1, and the emissivities are either considered uniform or are assigned specific values. In the infrared, the assigned values are $\varepsilon_{\lambda 1} = 0.985$ (typical of vegetation) and $\varepsilon_{\lambda 2} = 0.93$ (typical of bare soil) (Hipps (1989), van de Griend et al. (1 991). In the microwave, the emissivities are computed for specific values of soil moisture and vegetation water content. The temperature T_{s1} is fixed at 300 K, while T_{s2} is varied from 280-320 K such that the difference $\Delta T_{s1,2} = (T_{s2} - T_{s1})$ varies $\pm$ 20 °C. The positive range (up to +2o 'C) is typical of peak daytime temperature contrasts between bare and vegetated soil in semiarid environments (Humes et al. (1994)), while the negative temperature extreme (up to -2o 'C) is somewhat high for peak nighttime conditions but is included for the sake of illustration. The two components may be considered as separate and spatially distinct, with a single boundary between them, or as mixed, such as with patchy grasses or clumps of shrubs or trees.

The aggregation formula for emissivities (Eq. 14) is a simple area-weighting, hence the effective emissivity is the same as the composite emissivity, i.e. the difference $\Delta\overline{\varepsilon_\lambda} = \overline{\varepsilon_\lambda} - \overline{\varepsilon_\lambda}^*$ is zero. The interpretation of effective emissivity is therefore straightforward. Below, we focus mainly on interpreting the formulations for effect ive temperature,

(a) Infrared:

Eq. 16 is the aggregation formula for remotely sensed infrared effective surface temperature. Due to the nonlinearity of the Planck function, the infrared effective temperature differs from the composite temperature, i.e. $\Delta T_s = \overline{T}_s - T_s^* \neq O$. For the uniform emissivity case (i.e. $\varepsilon_{\lambda 1} = \varepsilon_{\lambda 2}$), Figures 1 (a) and 1 (b) show the dependence of $\Delta \overline{T}_s$ on the temperature contrast $\Delta T_{s1,2}$. The curves are shown for two different wavelengths, 12 μm and 9 pm, with fractional cover as a parameter. It is seen that $\Delta \overline{T}_s$ is always positive, i.e. the effective temperature is always greater than the composite temperature, and increases with magnitude of the component temperature contrast (the nonlinearity of the Planck function always biases the effective temperature towards the higher temperature component). $\Delta \overline{T}_s$ is largest for fractional cover ξ_1 near 0.5, and decreases to zero as expected for ξ_1 = O or 1, representing a homogeneous surface. This can be seen more clearly by plotting the curves versus fractional cover as in Figure 1 (c). The effects are not symmetrical with $\Delta T_{s1,2}$ or with ξ_1. The maximum value of $\Delta \overline{T}_s$ for the ranges shown is about 0.4 'C at 12 μm and 0.6 °C at 9 μm. The maximum value increases towards shorter wavelengths, and has a value of 1.7 °C in the 4 μm atmospheric window (not shown).

Figure 1 (d) shows the situation when the two components have different emissivities. The lower emissivity of tile simulated bare soil (component 2) has a compensatory effect for the bias towards its higher temperature- hence ΔT_s is lower for positive ΔT_{s12} than in Figure 1 (a). The converse is true for negative $\Delta T_{s1,2}$. In addition, $\Delta \overline{T}_s$ takes negative values over a portion of the range.

An implication of these results is that differences can be expected between remotely sensed (effective) surface temperatures and composite surface temperatures (such as used for validation purposes or as an assumption for remotely sensed surface temperatures in flux models). In the 10-12 μm region, and for naturally-occuring combinations of temperature and emissivity, three differences may range from a few to several tenths 'C— the specific values will depend also on the details of the multichannel algorithm used to retrieve the effective temperatures. One should consider carefully, therefore, the combinations of surface and observational conditions described here that give rise to the larger biases, especially at shorter wavelengths.

(b) Microwave:

For uniform emissivity, in the microwave case, Eq. 17 reduces to simple area-weighting. Thus, the microwave effective and composite surface temperatures are the same, and $\Delta\overline{T}_s = \overline{T}_s - \overline{T}_s^* = 0$.

In order to describe, somewhat realistically, the effects of nonuniform microwave emissivity, four cases of two-component surface types are considered as listed in Table 1. For each case, surface soil moisture and vegetation water content values are specified for each component, and corresponding emissivities are computed using Eqs. 8-10, assuming horizontal polarization and 20° zenith viewing angle, for wavelengths 24, 12, 6, and 3 cm. These wavelengths correspond to frequencies 1.25, 2.5, 5, and 10 GHz, which fall within the designated L, S, C, and X microwave wave-bands. The m and WC parameter contrasts between components 1 and 2 have been chosen to be reasonably realistic, and extreme cases have not been considered.

Figure 2 shows the dependence of $\Delta\overline{T}_s$ on temperature contrast $\Delta T_{s1,2}$ for each of the four cases. The curves in Figure 2(a) (Case 1) are plotted for different values of fractional cover ξ_1, (there is no modeled wavelength dependence in this case), while in Figures 2(b)-(d) (Cases 2-4) they are plotted for different wavelengths using a fixed value of $\xi_1 = .5$. As before, the differences $\Delta\overline{T}_s$ are largest for fractional cover $\xi_1 \cong .5$. The differences can take positive or negative values. The differences are positive when ΔT_{s12} is positive and the emissivity in component 2 is greater than that in component 1 (as expected from the form of Eq. 17). For a given temperature contrast $\Delta T_{s1,2}$, the difference $\Delta\overline{T}_s$ is largest when the emissivity contrast is greatest. This can occur at different wavelengths depending on the surface types. I-heterogeneous surfaces containing wet, bare soil and dense vegetation exhibit the largest emissivity contrasts and hence differences, $\Delta\overline{T}_s$. (The portions of the temperature contrast range, $\Delta T_{s1,2} = \pm 20$ °C, that are realistic to consider depend on the component surface types. No attempt is made here to limit the $\Delta T_{s1,2}$ values to realistic ranges for each case.)

Figure 3 shows the difference between effective and composite vegetation water contents, $\Delta\overline{W}_c$, based on Eqs. 20 and 22. The difference is always negative, indicating that the mean (area-averaged) vegetation water content over a heterogeneous footprint is underestimated in the microwave retrieval. The underestimation is greater for greater vegetation water contrasts, and for shorter wavelengths, at which the nonlinear effects of vegetation on microwave brightness temperature are greater. The effect is greatest at intermediate values of fractional cover, but there is increasing asymmetry as a function of fractional cover at shorter

wavelengths, biasing the occurence of the maximum difference towards smaller values of fractional cover of the lower-vegetation component.

Figure 4 shows the difference between effective and composite surface soil moisture contents, $\Delta\overline{m}$, based on Eqs. 21 and 22. In figures 4(a) and 4(b) the difference is shown as a function of fractional cover ξ_1 for values of moisture $m_1 = 0.1$ g cm^{-3} and $m_2 = 0.2$ g cm^{-3} in components 1 and 2 respectively, i.e. a value of $\Delta m_{1,2} = 0.1$ g cm^{-3}. Component 1 is bare soil, and the different curves correspond to increasing amounts of vegetation in component 2. The difference is quite small at 24-cm wavelength but increases to large values at shorter wavelengths. The difference is shown in Figures 4(c) and (d) as a function of moisture contrast, $\Delta m_{1,2}$, for fractional cover $\xi_1 = .5$.

5. Surface Flux Effective Parameters

We may contrast the expressions obtained in Section 3 with those derived for effective parameters applicable to flux modeling. One set of these, as derived by Chehbouni et al. (1995), are:

$$\overline{\varepsilon} = \sum_{i=1}^{N} \xi_i \varepsilon_i \tag{24}$$

$$\overline{T}_s = \frac{1}{\overline{w}} \sum_{i=1}^{N} \frac{\xi_i T_{si}}{w_i} \tag{25}$$

$$\frac{1}{\overline{w}} \cdot \sum_{i=1}^{N} \frac{\xi_i}{w_i} \tag{26}$$

$$\frac{1}{\overline{r}_a + \overline{r}_s} = \sum_{i=1}^{N} \frac{\xi_i}{r_{ai} + r_{si}} \tag{27}$$

where, ε, r_a, and r_s, were defined in Section 2.1, and w is a function of r_a and r_s and other surface parameters. We may note that while the expressions for effective emissivity (Eqs. 14 and 24) are the same, the expressions for effective surface temperature (Eqs. 16 or 17 and 25) are not. Chehbouni et al. show that the difference between effective temperature defined by Eq. 25 and composite temperature can range, for typical two-component surface contrasts, from approximately -4 to 1 'C. Future work should explore further the relationships between effective parameters

defined by remote sensing and those defined by flux aggregation, under realistic conditions, in order to improve he applicability of remote sensing data to surface flux studies.

6. Conclusions

In this paper, simplified radiative transfer models and two-component simulations have been used to show the effects of surface heterogeneity within the observation footprint on remotely sensed parameters in the thermal infrared and microwave spectral regions. The simulations have shown that remote sensing observations of heterogeneous terrain yield estimates of sensor-averaged, or "effective", parameters that may be significantly different from the simple area-averaged, or "composite", parameters that are often assumed to be estimated by the remote sensors. These differences arise from different sources in the infrared and microwave domains, but are a result in both cases of the nonlinear radiative transfer relationships between surface parameters and radiance received by the sensor. In the infrared case, for surface temperature sensing, the nonlinearity is caused by the Planck function. In the microwave case the nonlinearity is caused primarily by the vegetation opacity, such that the effective surface temperature, surface soil moisture, and vegetation water content always differ from their composite counterparts when vegetation is present. The magnitude of these differences depends on wavelength, the nonlinearities increasing in both infrared and microwave regions as the wavelengths decrease. The differences also depend on the relative fractional covers of the components and on their parameter contrasts, typically being largest at intermediate values of fractional cover. In many situations, the differences between effective and composite surface parameters may be small and can be safely neglected. However, in some cases, particular in semiarid environments or agricultural areas where large parameter contrasts exist between bare and vegetated surfaces, unexpectedly large differences may occur that need to be addressed.

The results obtained here use a simplified approach, and do not take into account the details of specific multichannel parameter retrieval algorithms or other practical issues such as variable instrument bandwidths, antenna beamwidths, atmospheric and instrument noise, multicomponent (more than two) footprints, and other factors. These should be the subject of further study. The results are indicative, however, of the magnitudes of nonlinear effects to be anticipated in estimating land surface

parameters over heterogeneous terrain. The results may also lead to further insights into the use of visible? and near-infrared (VNIR) remote sensing data, in combination with thermal infrared and microwave data, for estimating and monitoring surface fluxes. The VNIR data may provide information on vegetation fractional cover within the thermal infrared and microwave footprints, thus providing a means to correct for nonlinearities in the remotely sensed effective temperature, and to relate the remotely sensed effective temperature more closely to the effective temperature appropriate for large-area flux models.

6. Acknowledgments

This research was conducted at the Jet Propulsion Laboratory, California Institute of Technology, under contract with the National Aeronautics and Space Administration.

7. References

Becker, F. and Li, Z.-L. 1990, Towards a local split window method over land surfaces. *Int. J.* Rem. *Sens.*, 11 (3) 369-393.

Becker, F. and Li, Z.-L. 1994. Surface temperature and emissivity at various scales: definition, measurement and related problems. In: ***Proceedings of the Workshop on Thermal Remote Sensing of the Energy and Water Balance over Vegetation in Conjunction with Other Sensors, La Londe Les Maures, France, 20-23 September 1993,*** Cemagref Editions, Montpelier, France, 35-60.

Bougeault, P. 1991, Pararneterization schemes of land-surface processes for mesoscale atmospheric models. In: Schmugge, T.J. and Andre, J.-C. (eds). ***Land surface evaporation.*** Springer-Verlag, New York, 93-120.

Brutsaert, W. 1984. ***Evaporation into the atmosphere.*** Kluwer Academic Publishers, Dordrecht, The Netherlands.

Caselles, V. and Sobrino, J.A. 1989. Determination of frosts in orange groves from NOAA-9 data. ***Rem. Sens. Environ.,*** 29135-146.

Chehbouni, A., Njoku, E. G., Lhomrne, J. P., and Kerr, Y.H. 1995. Approaches for averaging surface parameters and fluxes over heterogeneous terrain. ***J. Climate, 8(5) 1386-1393.***

Choudhury, B.J., Tucker, C.J., Golus, R. E., and Newcomb, W.W. 1987. Monitoring vegetation using Nimbus-7 scanning multichannel microwave radiometer data. ***Int. J. Rem. Sens.***, 8(3) 533-538.

Dozier, J. 1981. A method for satellite identification of surface temperature fields of subpixel resolution. ***Rem. Sens. Environ.,*** 11221 -229.

Entekhabi, D., Nakamura, H., and Njoku, E.G. 1994. Solving the inverse problem for soil moisture and temperature profiles by the sequential assimilation of multifrequency remotely sensed observations. *IEEE* ***Trans. Geosci. Rem. Sens., 32438-448.***

Famiglietti, J. S., Wood, E. F., Sivapalan, M., and Thongs, D.J. 1992. A catchment scale water balance model for FIFE. J *Geophys. Res.*, 97(D 17) 18997-19007.

Goody, R.M. and Yung, Y.L. 1989. ***Atmospheric radiation. Theoretical basis.*** Oxford University Press, Oxford, UK.

Hipps, L.E. 1989. The infrared emissivities of soil and *Artemisia tridentata* and subsequent temoeratur corrections in a shrub-steppe ecosystem. ***Rem. Sens. Environ., 27337-342.***

Holwill, C.J. and Stewart, J.B. 1992. Spatial variability of evaporation derived from aircraft and ground-bed data. *J. Geophys. Res.*, 97(D17) 18673-18680.

Humes, K. S., Kustas, W.P., Moran, M. S., Nichols, W. D., and Weltz, M.A. 1994. Variability of emissivity and surface temperature over sparsely vegetated surfaces. *Water Resources Res.*, 30(5) 1299-1310.

Jackson, T.J. and Schmugge, T.J. 1991. Vegetation effects on the microwave emission of soils. ***Rem. Sens. Environ., 36203-212,***

Kealy, P.S. and Hook, S.J.]993. Separating temperature and emissivity in thermal infrared multispectral scanner data: Implications for recovering land surface temperatures. *IEEE Trans. Geosci. Rem. Sens.*, ***31(6) 1155-1164.***

Kerr, Y.H., Lagouarde, J.P., and Imbernon, J, 1992. Accurate land surface retrieval from AVHRR data with use of an improved split window algorithm. ***Rem. Sens. Environ.,*** 41197-209.

Kerr, Y.H. and Wigneron, J.P.]99s. Vegetation models and observations - a review. In: Choudhury, B.J., Kerr, Y. H., Njoku, E. G., and Pampaloni, P. (eds). ***Passive micro wave rem ote sensing of land-atmosphere interactions.*** VSP Utrecht, The Netherlands, 317-344.

Kustas, W. P., Choudhury, B.J., Moran, M. S., Reginato, R. J., Jackson, R.D., Gay, L. W., and Weaver, H.L. 1989. Determination of sensible heat flux over sparse canopy using thermal infrared data, *Agric. Forest Meteorol.*, 44 197-216.

Labed, J. and Stoll, M.P.]99]. Spatial variability of land surface emissivity in the thermal infrared band: Spectral signature and effective surface temperature. ***Rem. Sens. Environ., 381-17.***

Lo Seen, D., Chehbouni, A., Njoku, E., Saatchi, S., Mougin, F,., and Monteny, B. 1995. A coupled biomass production, water and surface energy balance model for remote sensing applications in semiarid grasslands. *Agric. Forest Meteorol.*, (submitted).

Njoku, E.G. 1995, Surface temperature estimation over land using satellite microwave radiometry. In: Choudhury, B,J., Kerr, Y. H., Njoku, E. G., and Pampaloni, P. (eds). ***Passive microwave remote sensing of land-atmosphere interactions.*** VSP Utrecht, The Netherlands, 509-530.

Njoku, E.G. and Entekhabi, D. 1995, Passive microwave remote sensing of soil moist ure. *J. Hydrology*, (in press),

Owe, M., van de Griend, A. A., and Chang, A.T.C. 1992, Surface moisture and satellite microwave observations in semiarid southern Africa. ***Water Resources Res.***, 28(3) 829-839.

Prata, A..J. 1993. Land surface temperatures derived from the Advanced Very High Resolution Radiometer and the Along-Track Scanning Radiometer 1. Theory. *J. Geophys. Res.,* 98(D9) 16689-16702.

Prevot, L., Brunet, Y., Paw U, K. T., and Seguin, B. 1994. Canopy modeling for estimating sensible heat flux from thermal infrared measurements. In: ***Proceedings of the Workshop on Thermal Remote Sensing of the Energy and Water Balance over Vegetation in Conjunction with Other Sensors, La Londe Les Maures, France, 20-23 September 1993,*** Cemagref Editions, Montpelier, France, 17-22,

Rowntree, P.R. 1991. Atmospheric parametrization schemes for evaporation over land: basic concepts and climate modeling aspects. In: Schmugge, T.J. and Andre, J.-C. (eds). ***Land surface evaporation.*** Springer-Verlag, New York, 5-29.

Running, S.W.1990. Estimating terrestrial primary productivity by combining remote sensing and ecosystem simulation. In: Hobbs, R. and Mooney, H. (eds). ***Remote sensing of biosphere functioning.*** Springer-Verlag, New York, 65-86,

Salisbury, J.W. and D'Aria, D. 1992. Emissivity of terrestrial materials in the 8-14 µm atmospheric window. ***Rem. Sens. Environ.,*** 4283-106.

Shuttleworth, W.J. 1991. The modellion concept. ***Rev.*** *Geophys.*, 29585-606,

Sobrino, J. A., Coil, C., and Caselles, V. 1991. Atmospheric correction for land surface temperature using NOAA-1 1AVI IRR channels 4 and 5. ***Rem. Sens. Environ.,*** 3819-34.

van de Griend, A. A., Owe, M., Green, M., and Stoll, M. I). 1991. Measurement and spatial variation of thermal infrared spatial emissivity in a savanna environment. *Water* ***Resources*** *Res.*, ***27371-379.***

Wan, Z. and Dozier, J. 1989. Land surface temperature measurement from space: Physical principles and inverse modeling. ***IEEE*** *Trans. Geosci.* ***Rem.*** *Sens.*, 27(3) 268-278.

Wang, J. R., O'Neil], P. E., Jackson, T.J., and Engman, E. I", 1983. Multifrequency measurements of the effects of soil moisture, soil texture, and surface roughness. ***IEEE Trans.*** *Geosci.* ***Rem,*** *Sens.*, ***GE-21 44-51.***

Tables

Table 1: Simulated two-component surfaces for analysis of effects of microwave-derived effective parameters. (W. is vegetation water content in kg m^{-2}; m is surface soil moisture in g cm^{-3}; ε_λ is modeled emissivity, where λ is wavelength in cm)

Case #	Component	Description	WC	m	ε_{24}	ε_{12}	ε_{6}	ε_{3}
1	1	Moist soil	O	.1	.795	.795	.795	.795
	2	Dry soil	0	.05	.870	.870	.870	.870
2	1	Grass	.5	.1	.804	.812	.828	.856
	2	Dry soil	0	.05	.870	.870	.870	.870
3	1	Crops	2	.1	.828	.856	.899	.950
	2	Dry soil	0	.05	.870	.870	.870	.870
4	1	Crops	2	.2	.703	.751	.825	.914
	2	Wet soil	0	.15	.720	.720	.720	.720

Figures

Figure 1.

Difference $\Delta\overline{T}_s$ (°C), at infrared wavelengths, between effective (remotely sensed) and composite surface temperatures for a two-component surface: (a) as a function of temperature contrast $\Delta T_{s1,2}$ between the two components, for uniform emissivity and a wavelength of 12 μm---curves are shown for different values of fractional cover ξ_1 of component 1; (b) same as (a), but for a wavelength of 9 μm; (c) same as (a), but shown as a function of fractional cover ξ_1, with temperature contrast $\Delta T_{s1,2}$ as a parameter; (d) same as (a), but for components with different emissivities---$\varepsilon_{\lambda 1}$ = 0.985 (typical of vegetation) and $\varepsilon_{\lambda 2}$ = 0.93 (typical of bare soil).

Figure 2.

Difference $\Delta\overline{T}_s$ (°C), at microwave wavelengths, between effective (remotely sensed) and composite surface temperatures for a two-component surface, displayed as a function of temperature contrast $\Delta T_{s1,2}$ between components. The emissivity contrasts between components for each case are given in Table 1, Values shown are for horizontal polarization at a zenith viewing angle of 20°. (a) Case 1: shown for different values of fractional cover ξ_1 of component 1. (b) Case 2: shown for different wavelengths and for fractional cover ξ_1 = 0.5. (c) Case 3: shown as in (b). (d) Case 4: shown as in (b).

Figure 3.

Difference $\Delta\overline{W}_c$ (kg m^{-2}), at microwave wavelengths, between effective (remotely sensed) and composite vegetation water contents for a two-component surface: (a) as a function of fractional cover ξ_1, with vegetation water content contrast $\Delta W_{c1,2}$ as a parameter, at a wavelength of 24 cm; (b) same as (a) but for a wavelength of 3 cm; (c) as a function of vegetation water content contrast $\Delta W_{c1,2}$, with wavelength as a parameter, and fractional cover ξ_1 = 0.5.

Figure 4.

Difference $\Delta\overline{m}$ (g cm^{-3}), at microwave wavelengths, between effective (remotely sensed) and composite surface soil moisture contents for a two-component surface: (a) as a function of fractional cover ξ_1, for soil moisture contrast $\Delta m_{1,2}$ = 0.1 g cm^{-3}, with vegetation water content contrast $\Delta W_{c1,2}$ as a parameter, and a wavelength of 24 cm; (b) same as (a) but for a wavelength of 3 cm; (c) as a function of soil moisture contrast $\Delta m_{1,2}$, with vegetation water content contrast $\Delta W_{c1,2}$ as a parameter, for fractional cover ξ_1 = 0.s, and a wavelength of 24 cm; (d) same as (c) but for a wavelength of 3 cm.

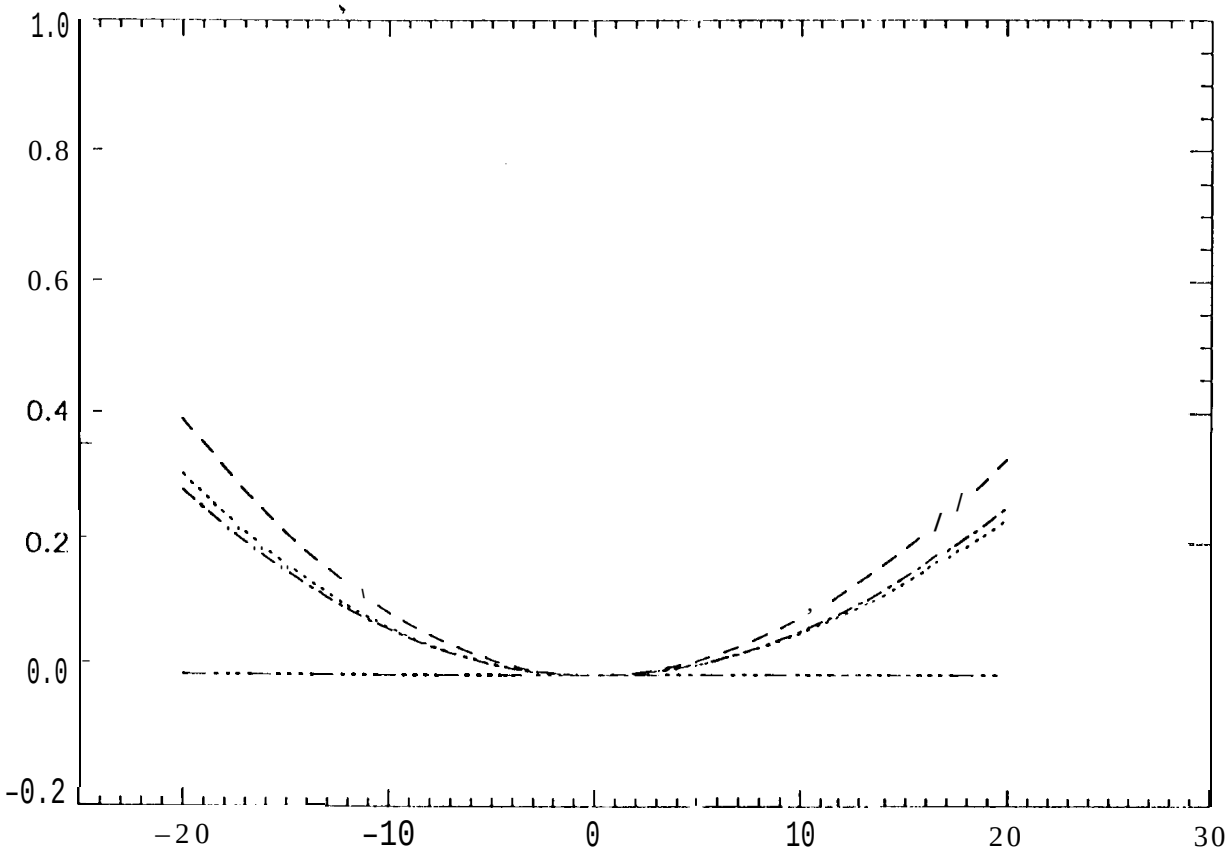

$\Delta T_{s_{1,2}} = (T_{-,-} T_{,})$

$\varepsilon_1 = \varepsilon_2 = 1$

$\lambda = 12\mu$

..... $\xi_1 = 0.25$

– – – – – $\xi_1 = 1.73$

—, ----- . $\xi_{1} = 0.75$

—..,—... $\xi_1 = 0.1$

Fig 1(a)

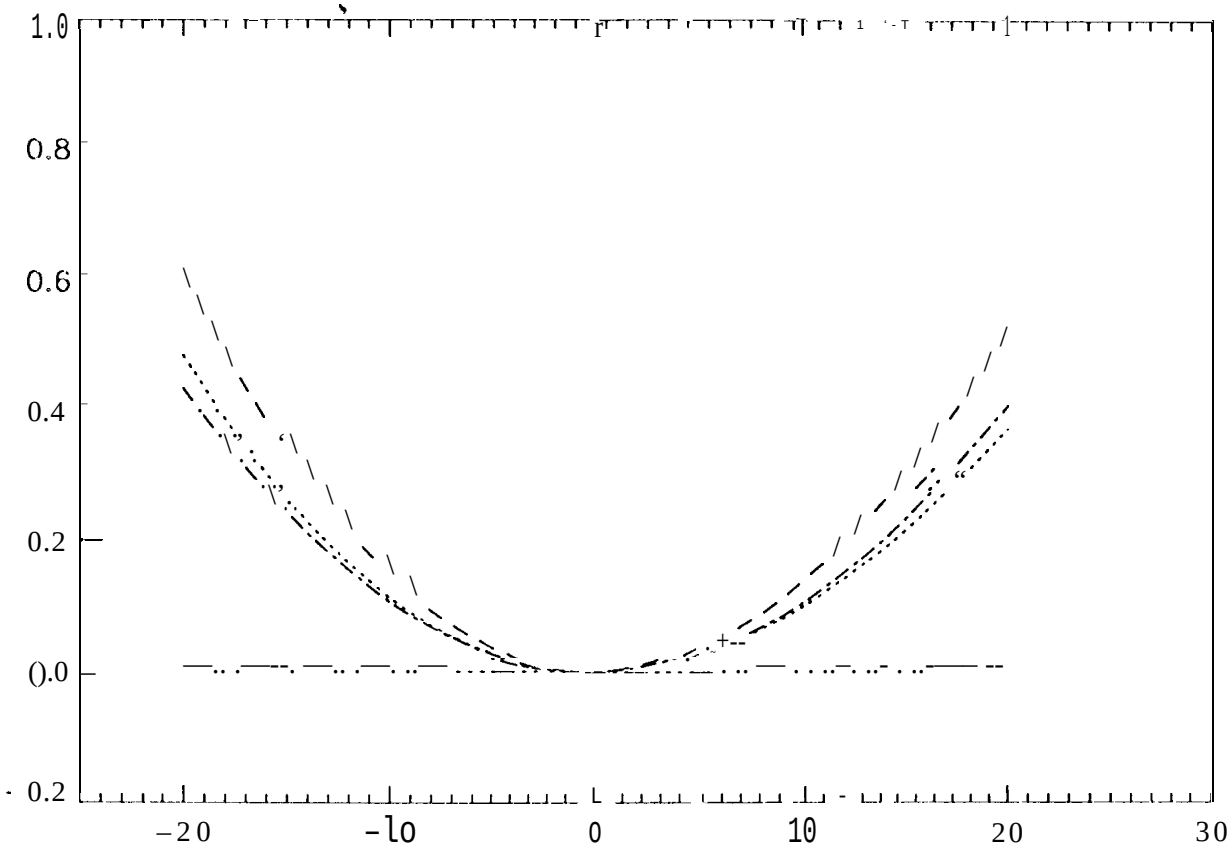

$\Delta \bar{T}_s$

$\Delta T_{s_{1,2}} = (T_2 - T_1)$

$\varepsilon_1 = \varepsilon_2 = 1$

$\lambda = 9\mu$

..... $\xi_1 = 0,25$

---- -- $\xi_1 = 0.5$

-.-.-. $\xi_1 = 0.75$

—.—.—. $\xi_1 = 0,1$

Fig 1(b)

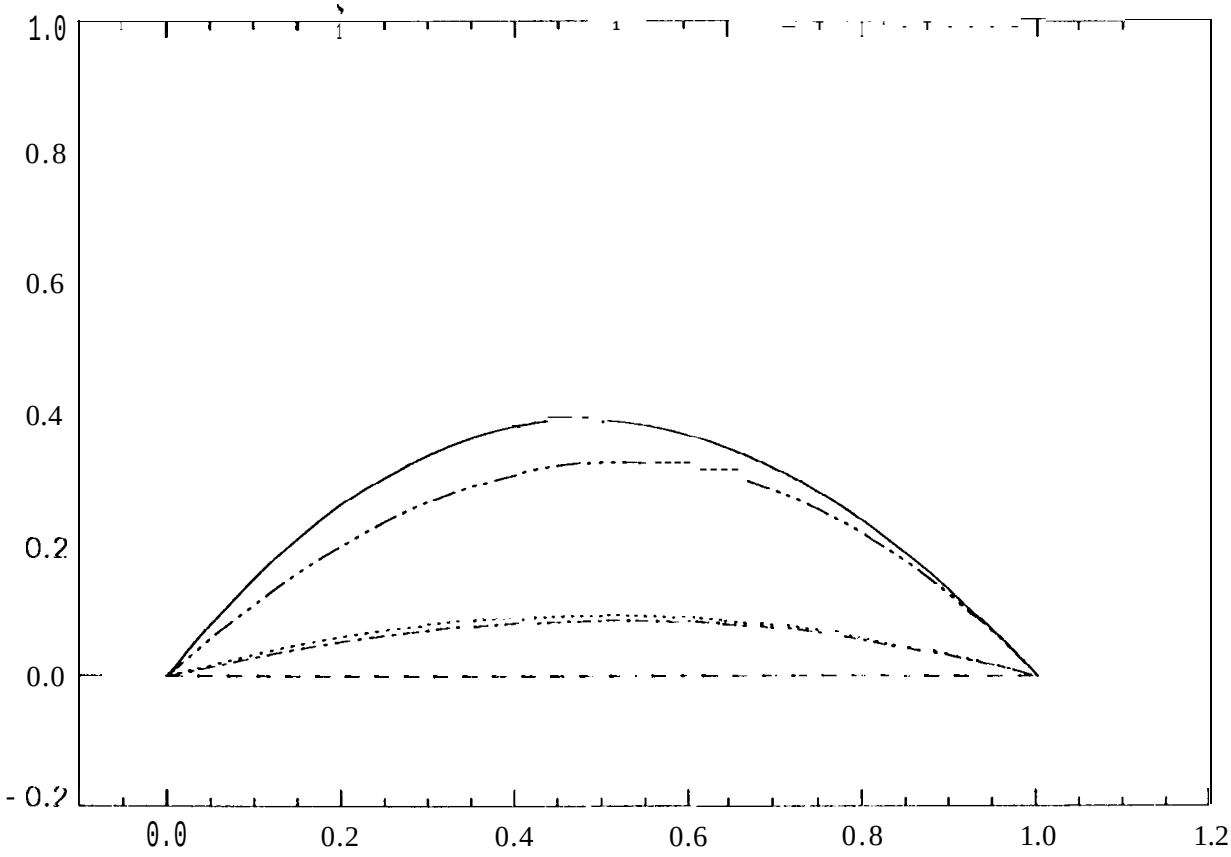

$\Delta \bar{T}_s$

Fractional Cover, ξ_1

$\varepsilon_1 = \varepsilon_2 = 1$

$\lambda = 12\,\mu$

$\Delta T_{s_{1,2}}$

- $(T_2 - T_1) = -20\,^\circ C$
- $(T_2 - T_1) = -10\,^\circ C$
- $(T_2 - T_1) = 0\,^\circ C$
- $(T_2 - T_1) = 10\,^\circ C$
- $(T_2 - T_1) = 20\,^\circ C$

Fig 1(c)

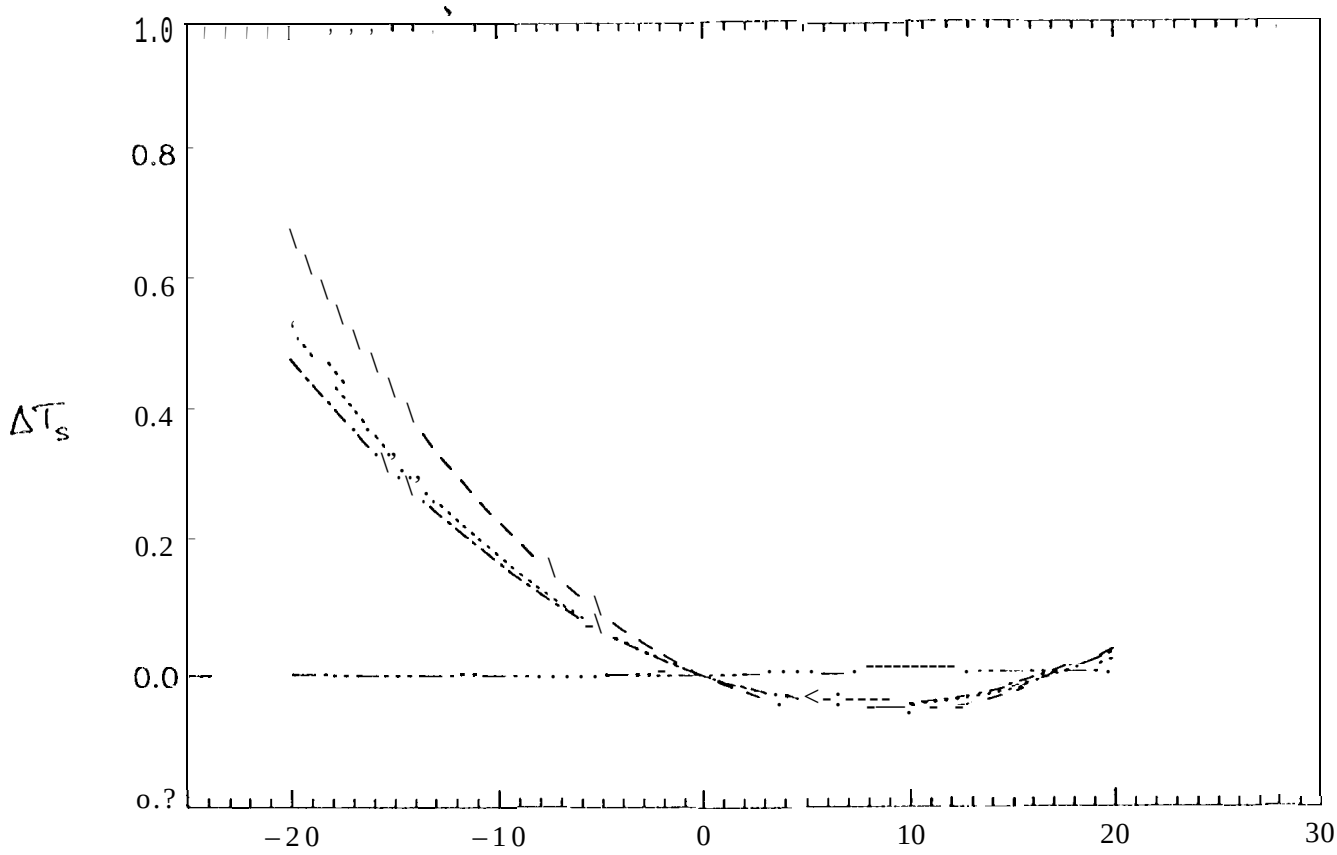

$\Delta T_{s_{1,2}} = (T_2 - T_1)$

$\varepsilon_1 = 0.985$

$\varepsilon_2 = 0.96$

$\lambda = 12\mu$

$\varepsilon_1 = 1$ 0,2s

$\varepsilon_1 = 0.5$

$\varepsilon_1 = 0.75$

$\varepsilon_1 = 0,1$

Fig 1(d)

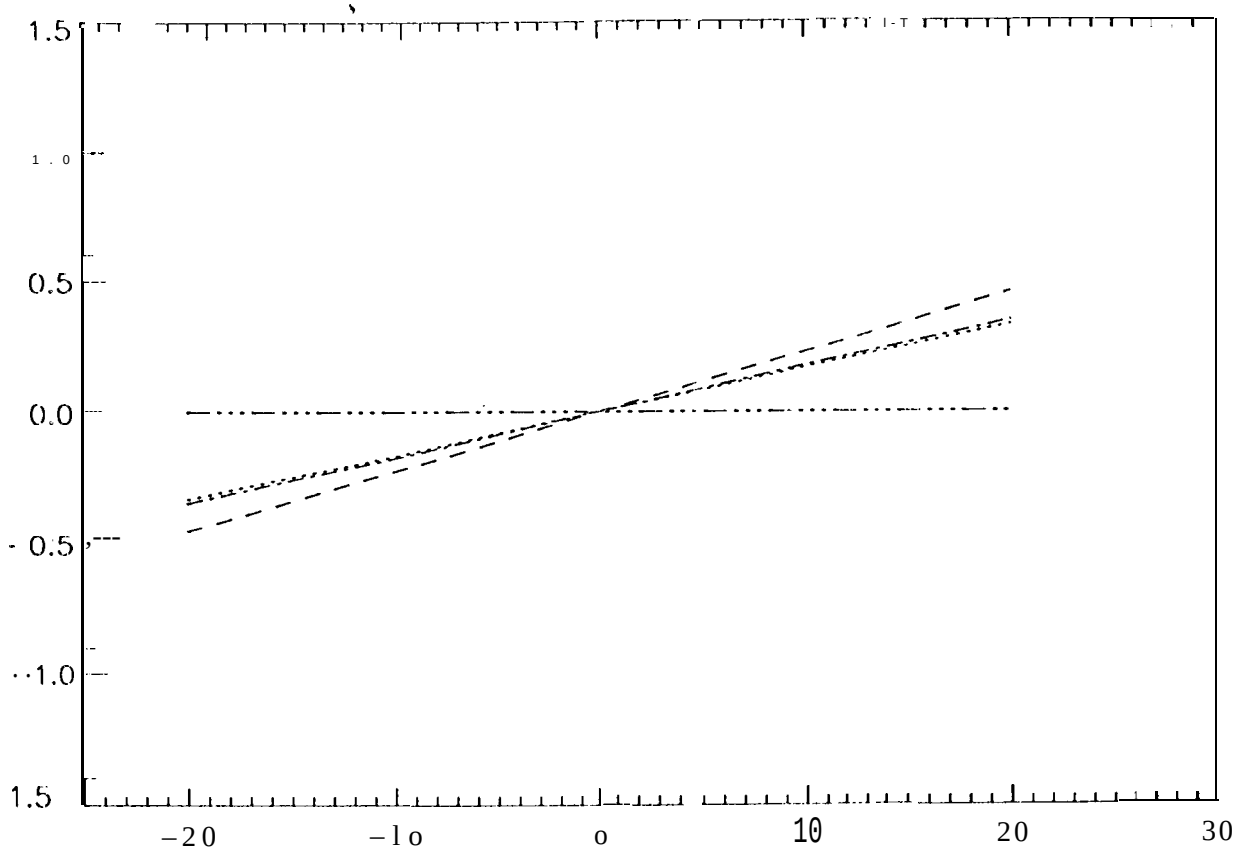

ΔT_s

$\Delta T_{s_{1,2}} = (T_2 - T_1)$

..... $\xi_1 = 0.25$

---- $\xi_1 = 0.5$

-.-.-.- $\xi_1 = 0.75$

-...-... $\xi_1 = 0.1$

Fig 2(a)

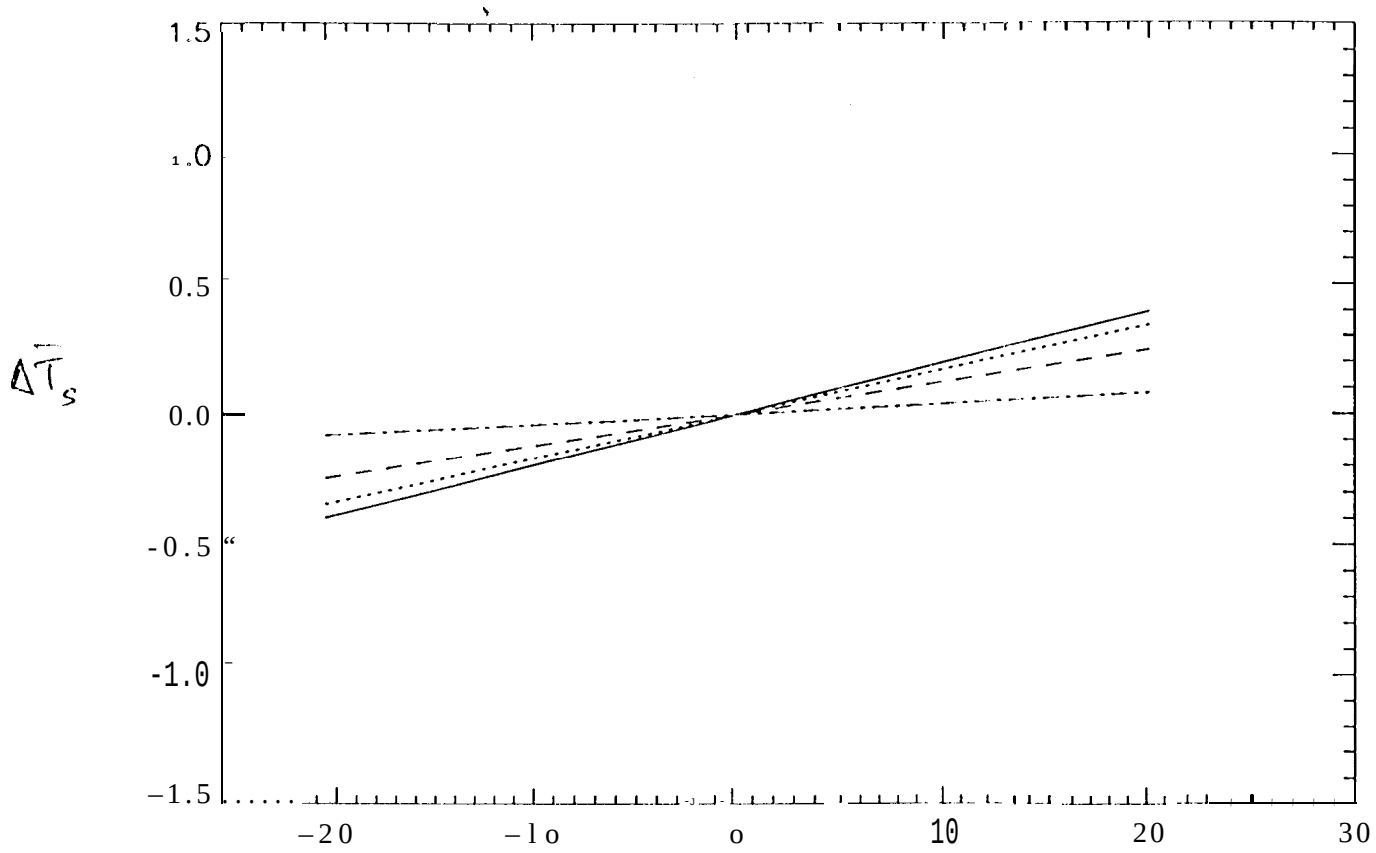

$$\Delta \bar{T}_{s_{1,2}} = (\bar{T}_2 - \bar{T}_1)$$

$\xi_1 = 0.5$

——— $\lambda = 24$ cm

..... $\lambda = 12$ cm

.. --- - $\lambda = 6$ cm

—.—.—.— $\lambda = 3$ cm

Fig 2(b)

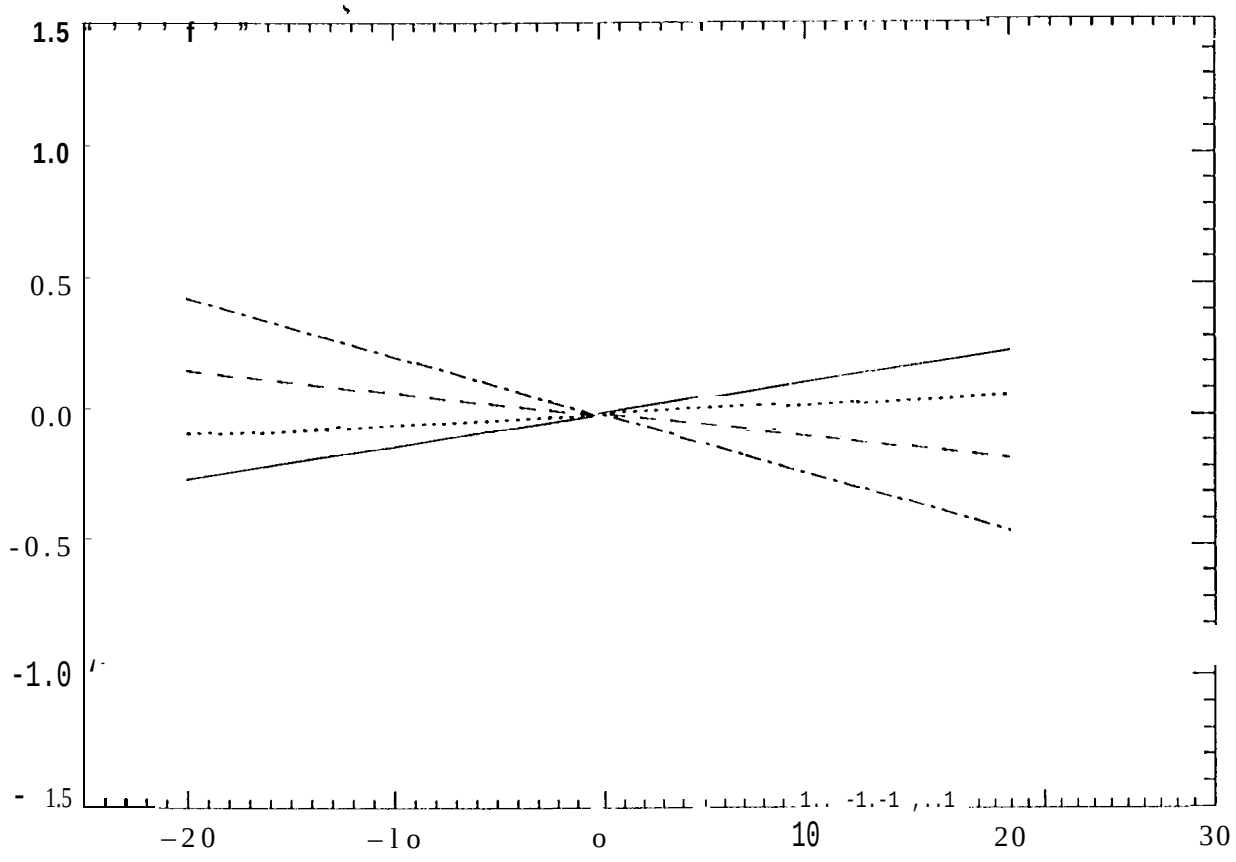

$\Delta \bar{T}_s$

$\Delta \bar{T}_{s_{1,2}} = (T_2 - T_1)$

$\xi_1 = 0.5$

——— $\lambda = 24$ cm

..... $\lambda = 12$ cm

– – – – $\lambda = 6$ cm

–·–·–·– $\lambda = 3$ cm

Fig 2(c)

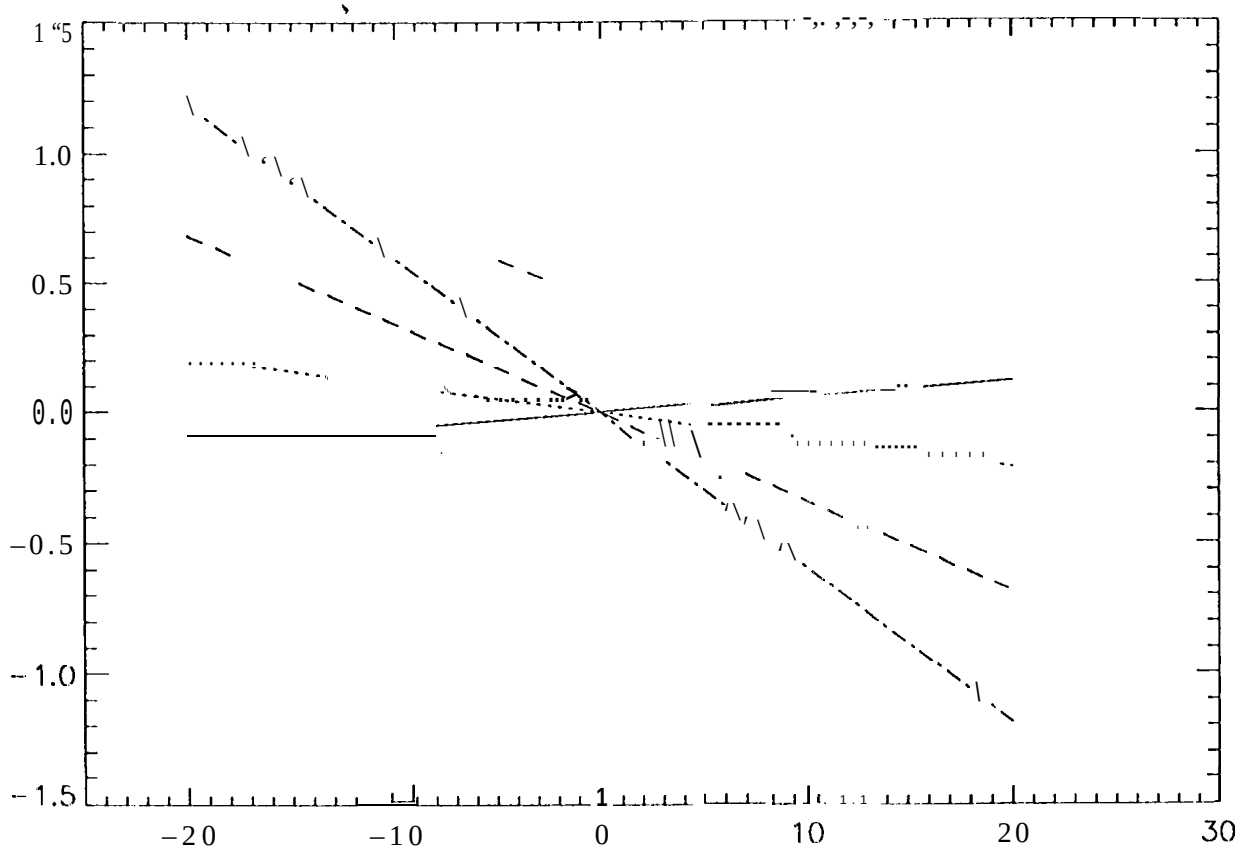

$\xi_1 = 0.5$

——— $\lambda = 24$ cm

····· $\lambda = 12$ cm

– – – – $\lambda = 6$ cm

–·–·–·– $\lambda = 3$ cm

Fig 2(d)

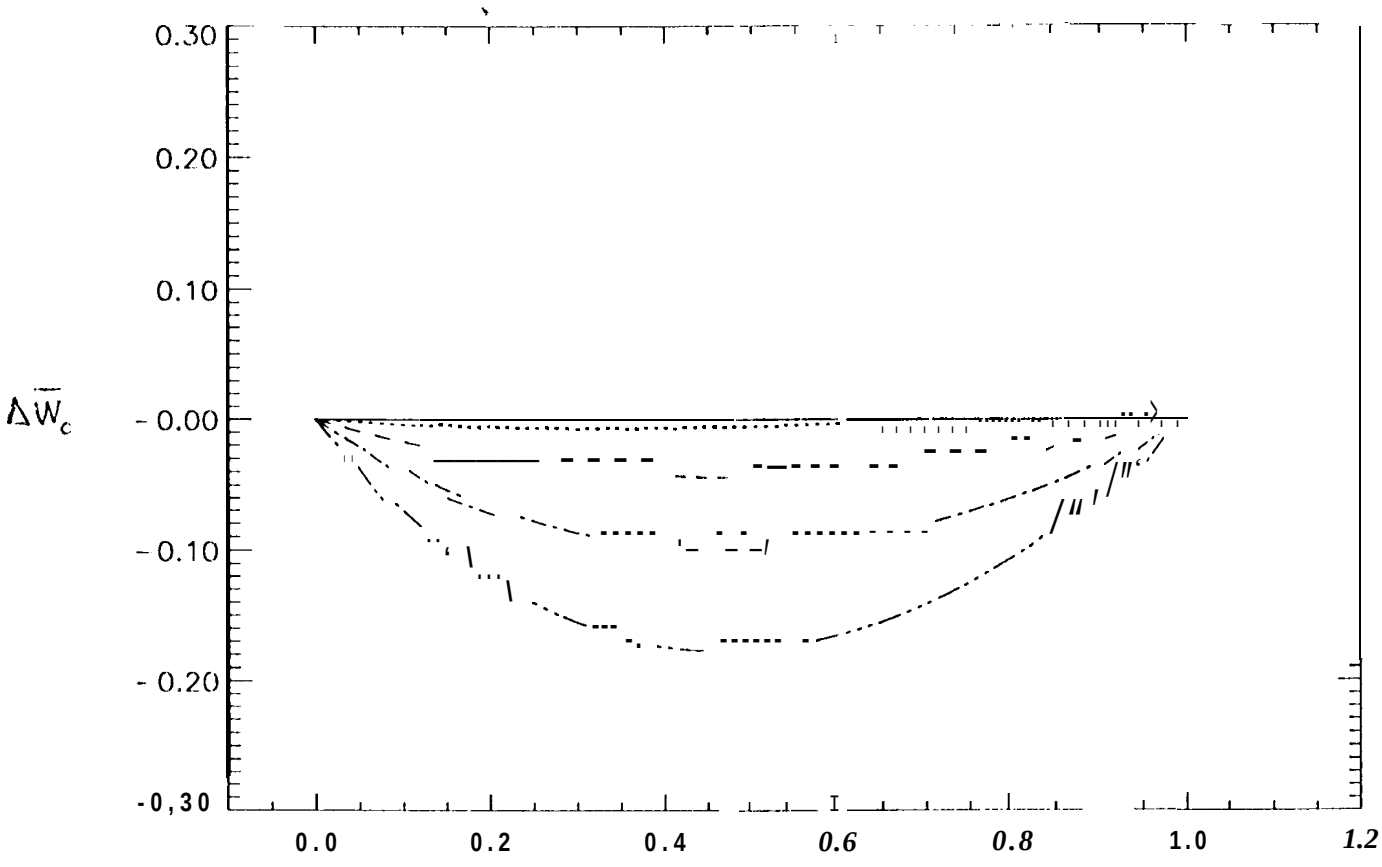

$\lambda = 24$ cm

($f = 1.25$ GHz)

$\Delta W_{1,2}$

———	$(W_2 - W_1) = 0$	kgm^{-2}
.....	$(W_2 - W_1) = 1$	"
– – – –	$(W_2 - W_1) = 2$	"
–.–.–.–	$(W_2 - W_1) = 3$	"
–..–..–	$(W_2 - W_1) = 4$	"

Fig 3(a)

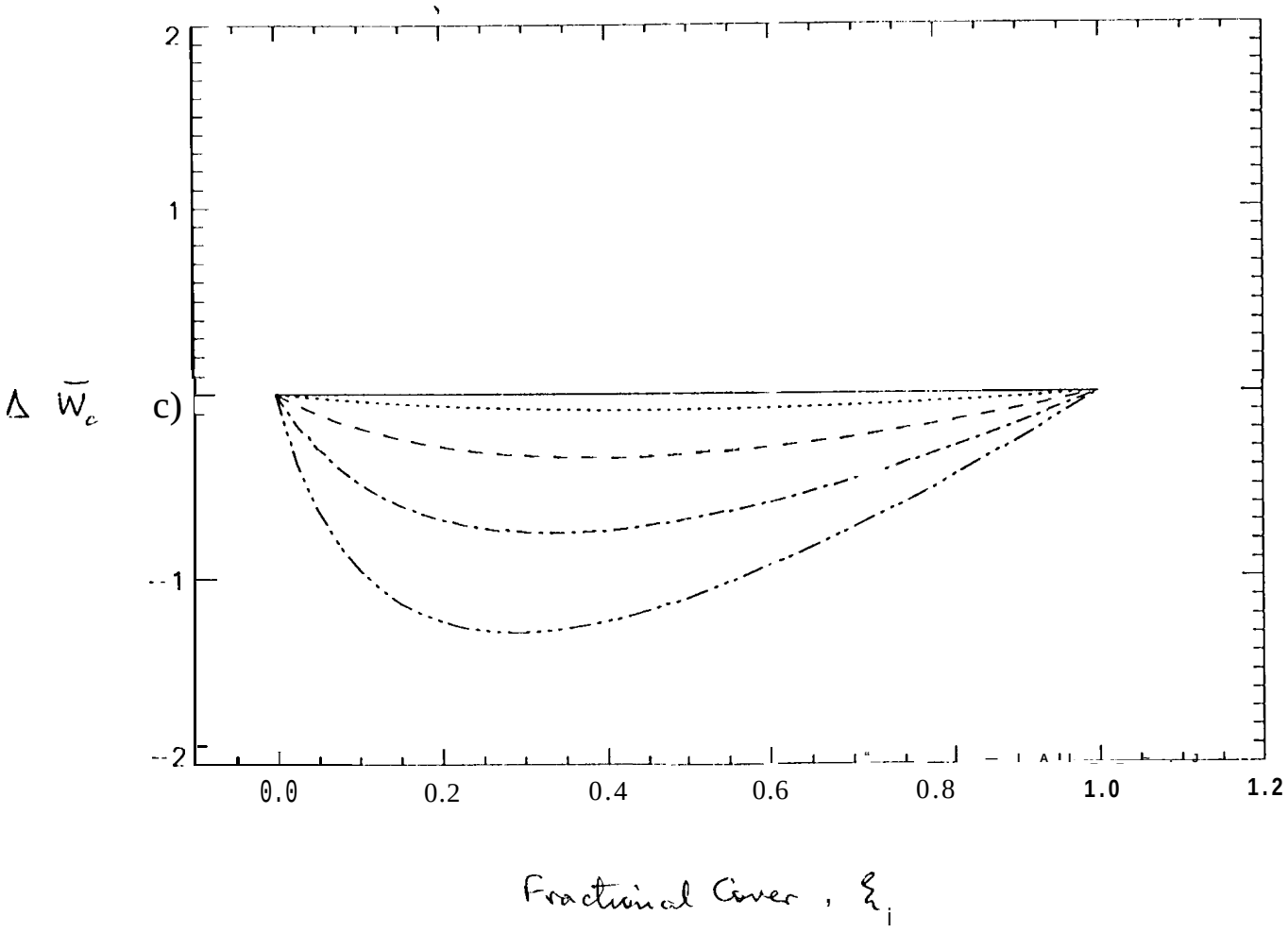

$\Delta \bar{W}_c$

$\lambda = 3cm$

$(f = 10\,GHz)$

$\Delta W_{1,2}$

——— $(W_2 - W_1) = 0$ kg m^{-2}

····· " = 1 "

– – – – – " = 2 "

·· — · — " = 3 "

····· — " = 4 "

Fig 3(6)

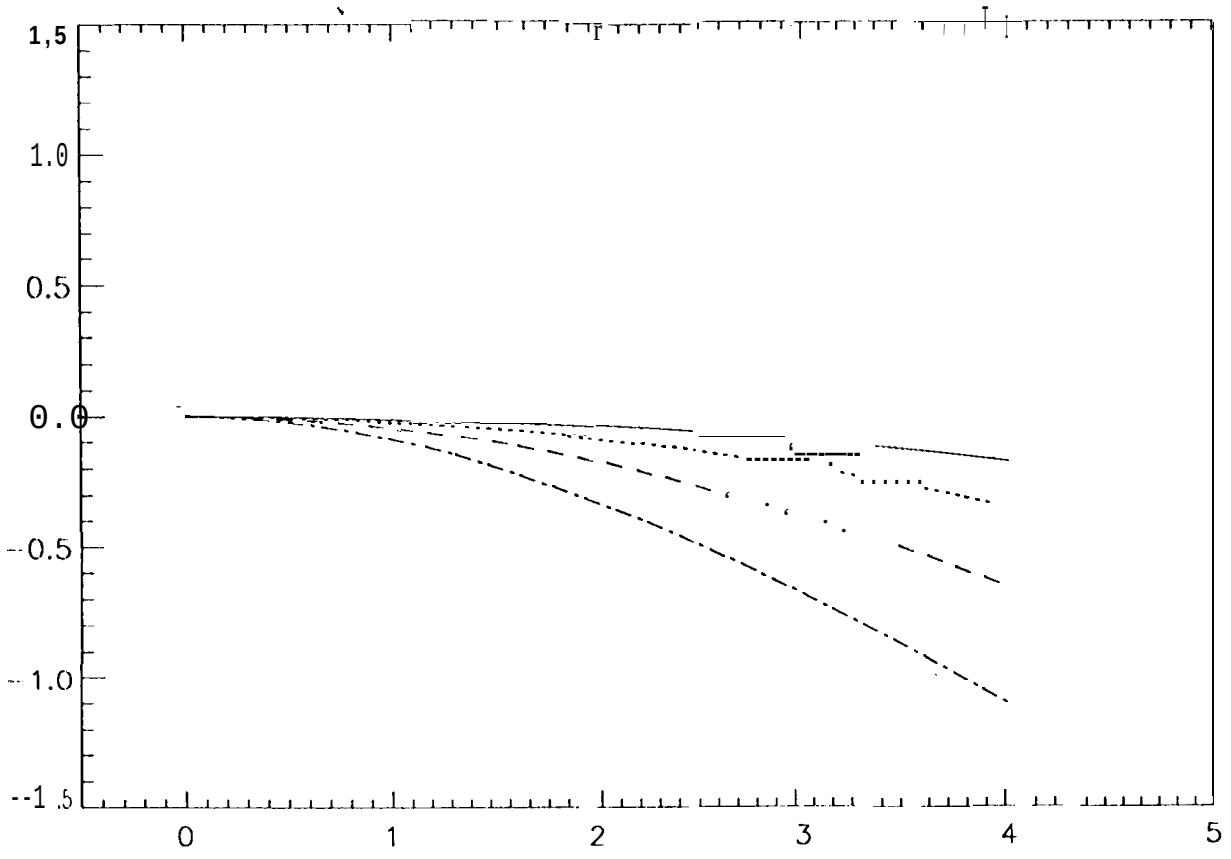

$\Delta \bar{W}_c$

$\Delta W_{1,2} = (W_2 - W_1)$ kg m^{-2}

$q = 0.5$

——— $\lambda = 24$ cm (1.25 GHz)
"""""""""" $\lambda = 12$ " (2.5 ")
– – – – – $\lambda = 6$ " (5.0 ")
– · – · – $\lambda = 3$ " (10.0 ")

Fig 3(c)

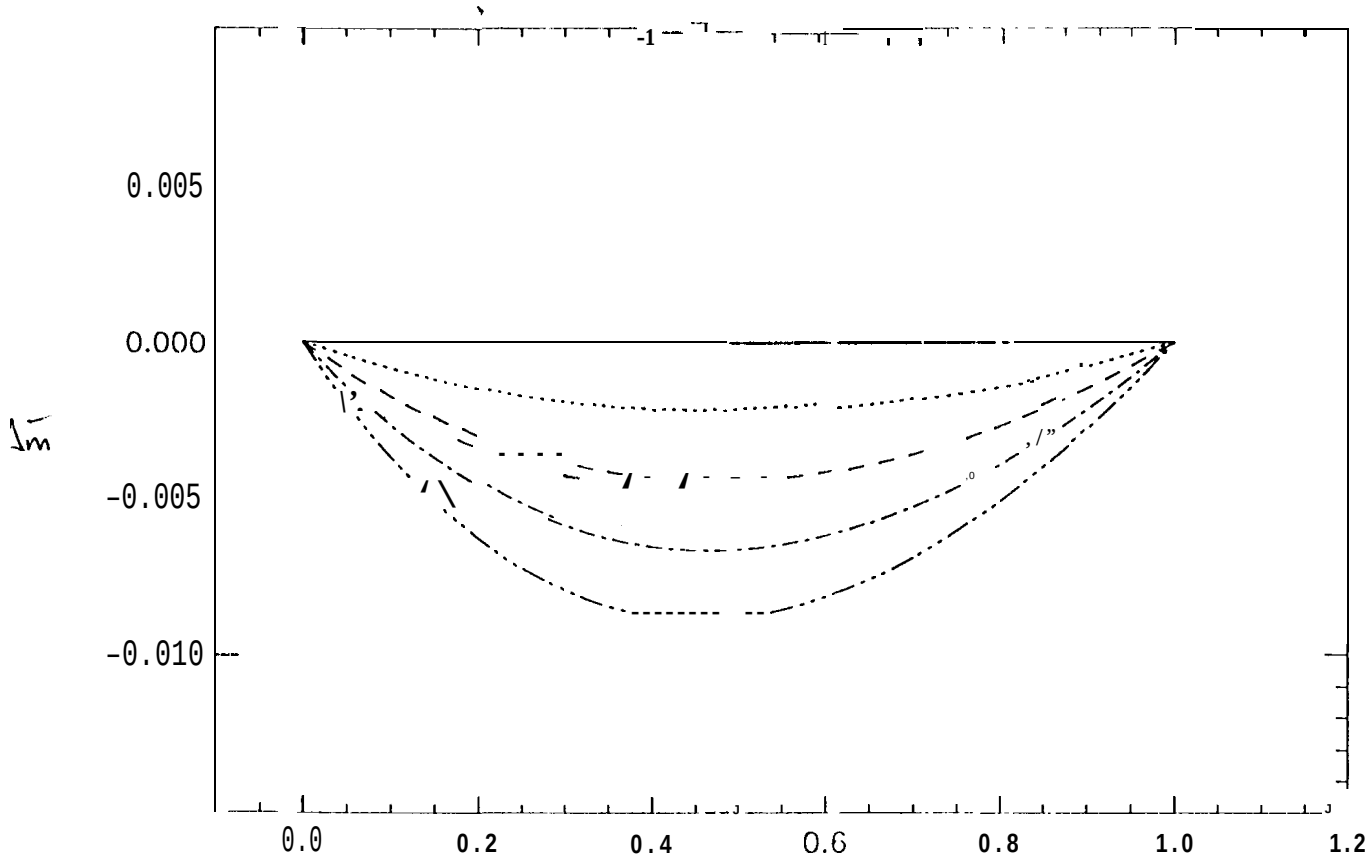

$m_1 = 0.1\ g\ cm^{-3}$

$m_2 = 0.2\ g\ cm^{-3}$

$\lambda = 24\ cm$

$\theta = 20°$

$W_{c_1} = 0\ kg\ m^{-2}$

——— $\Delta W_{c_{1,2}} = 0\ kg\ m^{-2}$

..... " = 1 "

- - - - - " = 2 "

-.-.-.- " = 3 "

—..... = 4 "

Fig 4(a)

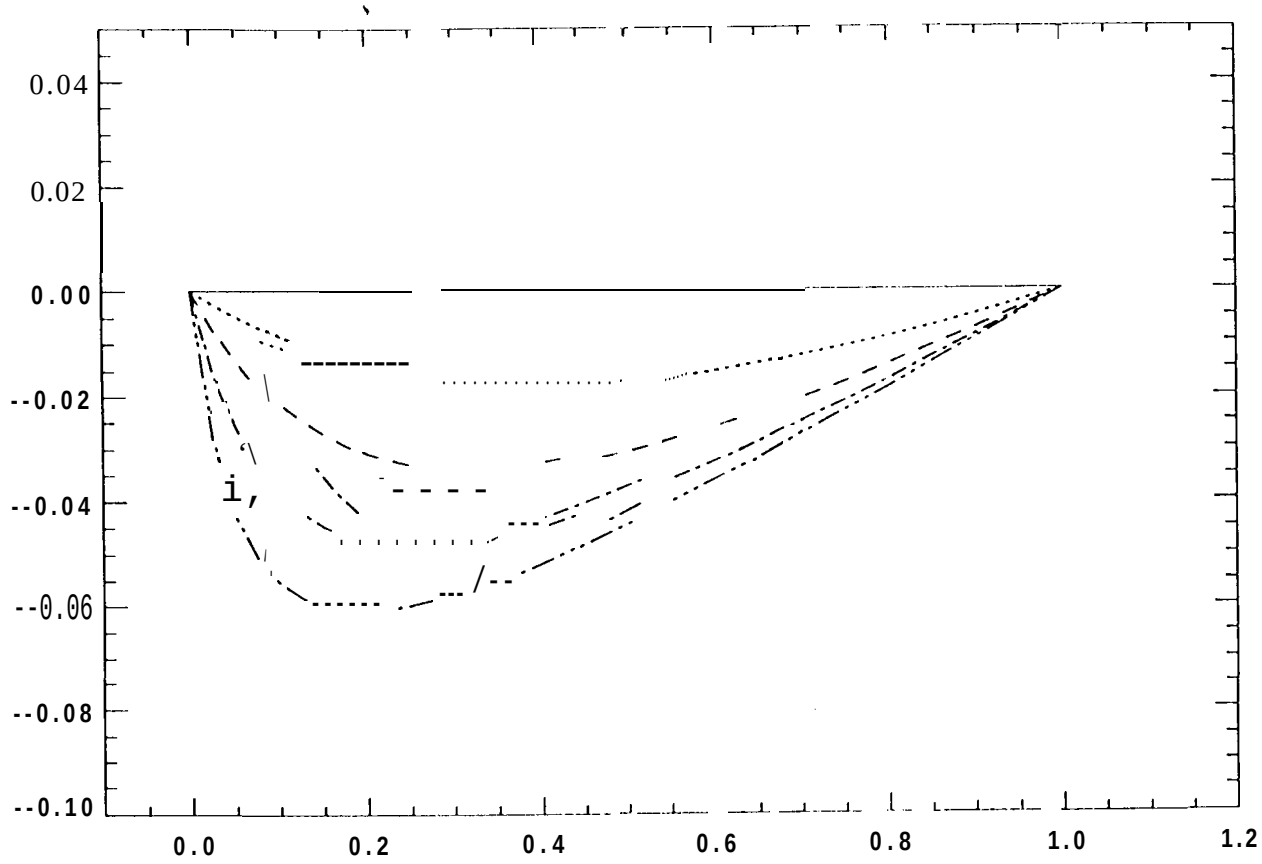

$m_1 = 0.1\ g\ cm^{-3}$

$m_2 = 0.2\ g\ cm^{-3}$

$\lambda = 3\ cm$

$\theta = 20°$

$W_{c_1} = 0$

——— $\Delta W_{c_{1,2}} = 0\ kg\ m^{-2}$

..... " = 1 "

– – – – – " = 2 "

-.-.-.- " = 3 "

-..-..- " = 4 "

Fig 4(b)

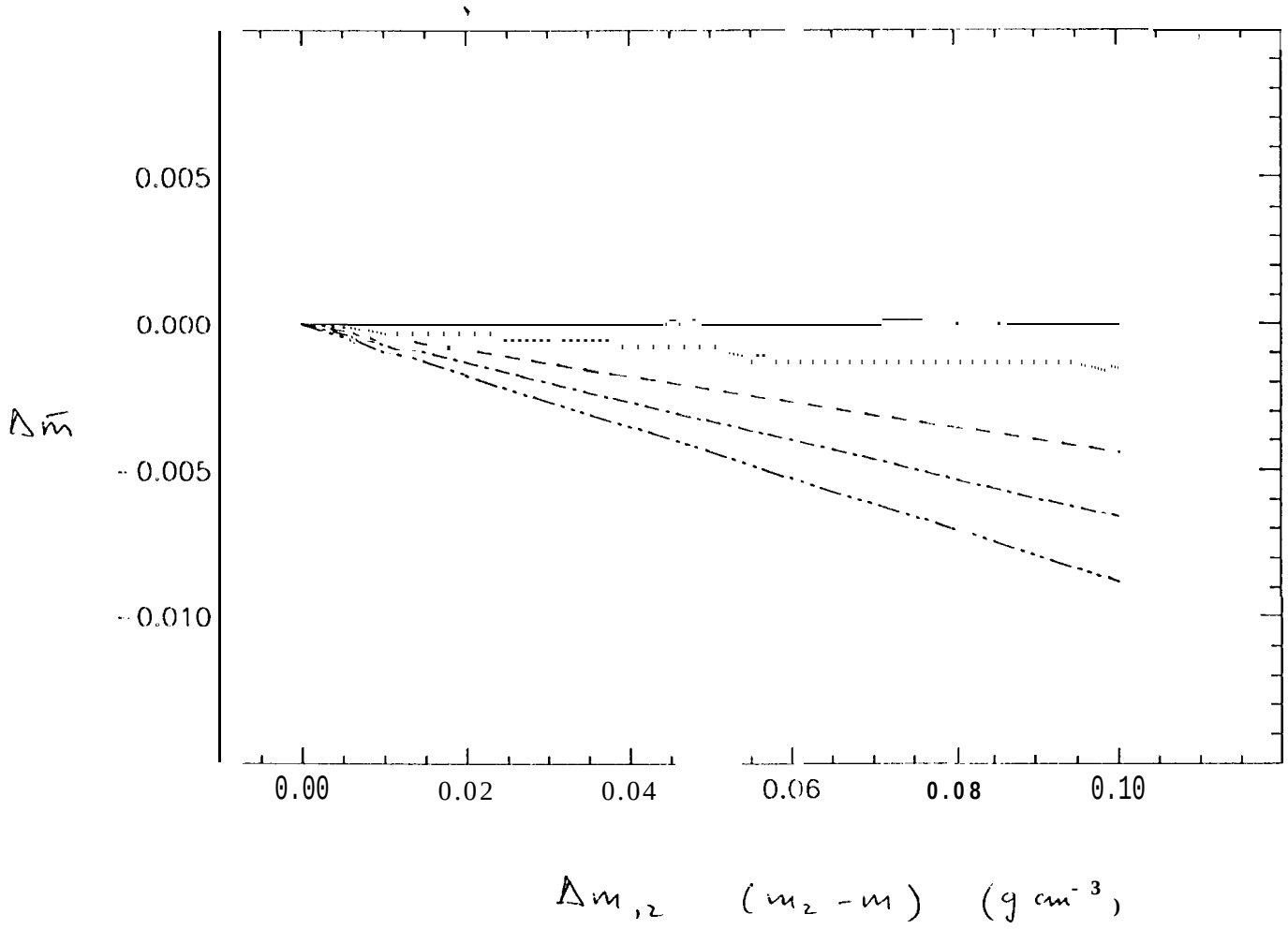

——— $\Delta W_{c_{1,2}} = 0$ 4 m^{-2}

..... " = 1 "

– – – – – " = 2 "

–·–·–·– " = 3 "

–··–··–·· " = 4 "

$\lambda = 2.4\ cm$

$\theta = 20°$

$W_{c_1} = 0\ kg\ m^{-2}$

$m_1 = 0.1\ g\ cm^{-3}$

Fig 4(c)

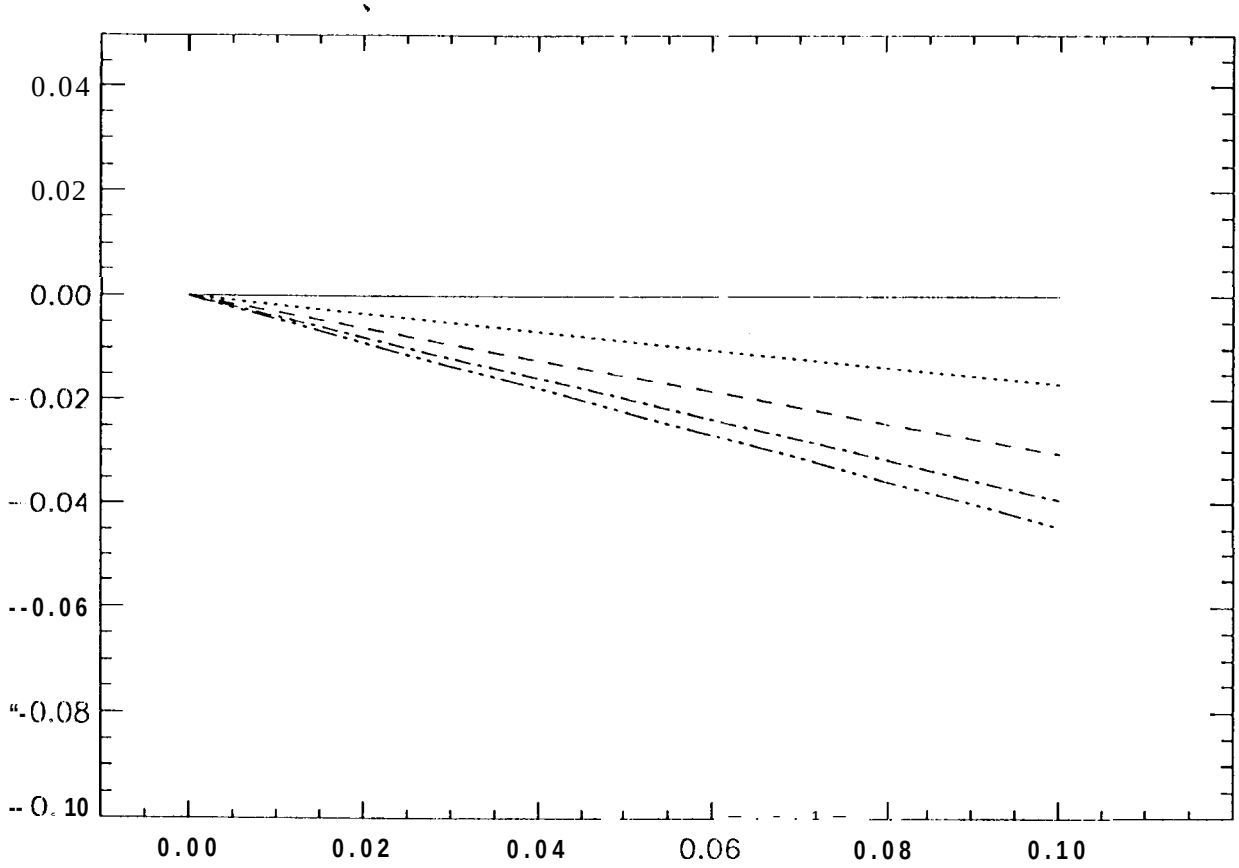

$\Delta \bar{m}$

$\Delta m_{1,2} = (m_2 - m_1$ $(g\ cm^{-3})$

$\lambda = 3cm$

$\theta = 20°$

$W_{c_1} = 0\ kg\ m^{-2}$

$m_1 = 0.1\ g\ cm^{-3}$

——— $\Delta W_{c_{1,2}} = 0\ kg\ m^{-2}$

..... " = 1 "

– – – – – " = 2 "

–·–·– " = 3 "

–··–··– " = 4 "

Fig 4(d)